International Forum on Aeroelasticity and Structural Dynamics
IFASD 2017
25-28 June 2017, Como - Italy

INDUSTRIAL FREQUENCY-DOMAIN LINEARIZED NAVIER-STOKES CALCULATIONS FOR AEROELASTIC PROBLEMS IN THE TRANSONIC FLOW REGIME

Laurent Daumas[1], Nicolas Forestier[2], Aloïs Bissuel, Gabriel Broux, Frédéric Chalot, Zdenek Johan and Michel Mallet

DASSAULT AVIATION
78 quai Marcel Dassault, 92552 Saint-Cloud Cedex, France

[1] laurent.daumas@dassault-aviation.com
[2] nicolas.forestier@dassault-aviation.com

Keywords: linearized CFD, turbulence gradient, HPC scalability, large-scale computations

Abstract: Linearized CFD solvers are commonly used at DASSAULT AVIATION to predict unsteady aerodynamic pressure fields on an aircraft in the transonic flow regime. This paper shows that accounting for the gradient of the Reynolds stress tensor is of major importance to predict the aerodynamic behavior of the aircraft from subsonic to transonic domain (including separated flows). This paper presents the strategy used to develop an approach coupling the linearized Navier-Stokes equations and the linearized turbulent system in the frequency-domain based on the in-house finite element *AETHER* code. The turbulence modelling is achieved through the Spalart-Allmaras model. This coupled approach is validated using data of a wind tunnel campaign performed at ONERA S2MA and by comparison with time-domain non-linear computations. Finally, the industrial capability of the frequency-domain linearized Navier-Stokes solver with linearized turbulence is illustrated through applications on the FALCON 7X and RAFALE fighter.

1 INTRODUCTION

DASSAULT AVIATION aeroelastic tools allow an efficient coupling of several CFD approaches (linearized frequency-domain, non-linear time-domain and Detached Eddy Simulation Navier-Stokes) of the in-house flow solver *AETHER* with every component of the structural solver ELFINI. This powerful capability is used routinely for on-going aircraft programs such as FALCON business jets or weapon store integration on the RAFALE fighter jet.

This paper deals with the strategy implemented at DASSAULT AVIATION to predict more accurately unsteady aerodynamic pressure fields on an aircraft in the transonic flow regime. In this regime, aeroelastic analysis becomes significantly more complex: shock waves appear and disappear due to aircraft deformations, separated flows can be observed as these shocks move rearward on the aircraft lifting surfaces and global aerodynamic coefficients can vary significantly over the Mach number range.

These transonic phenomena have an effect on the aeroelastic behavior of the aircraft. Consequently, linearized CFD solvers are routinely used at DASSAULT AVIATION in

addition to Doublet Lattice Methods to predict unsteady aerodynamic pressure fields on an aircraft in the transonic flow regime [1]. The account for the derivative of the Reynolds stress tensor has been proven to be of major importance to predict properly the behavior of the shock/boundary layer interaction at high Mach numbers [2].

Computational cost reductions have been achieved for the resolution of the linear system resulting from the frequency-domain formulation by means of a preconditioned GMRES solver. Efficient massively parallel implementation has also been developed and typical computations are now performed on parallel computers using 500 to 4000 cores. The *industrial* use of this frequency-domain linearized CFD approach is now possible, as opposed to a non-linear time-domain approach.

2 NON-LINEAR NAVIER-STOKES SOLVER

DASSAULT AVIATION Navier-Stokes *AETHER* code solves the 2D, axisymmetric, and 3D compressible Navier-Stokes equations. It uses a finite element approach, based on a symmetric form of the equations written in terms of entropy variables. The advantages of this change of variables are numerous: in addition to the strong mathematical and numerical coherence they provide (e.g., dimensionally correct dot product, symmetric operators with positivity properties, and efficient preconditioning), entropy variables yield further improvements over the usual conservation variables, in particular in the context of chemically reacting flows.

The code can handle the unstructured mixture of numerous types of elements (triangles and quadrilaterals in 2D; tetrahedra, bricks, and prisms in 3D). It has been successfully ported on many computer architectures. It is fully vectorized and parallelized for shared or distributed memory machines using the MPI message passing library (IBM PureFlex and Blue Gene/Q, Bull bullx).

Several one- and two-equation Reynolds-averaged turbulence models are available: Spalart-Allmaras, K-ε, K-ω, K-ℓ, K-KL… These models are integrated down to the wall. Extensions to LES and DES are also available.

3 LINEARIZED NAVIER-STOKES EQUATIONS

On one side, the state equation described by the Navier-Stokes equations in the Arbitrary Lagrangian Eulerian formulation can be formally expressed by [3]

$$E\left(V, \dot{V}, \mu_t, x, w\right) = 0 \tag{1}$$

with V the entropy variables, μ_t the turbulent viscosity, x the coordinates, and w the mesh velocity (upper dots denote time derivatives).

The linearization of the eq. (1) gives to the first order:

$$\frac{\partial E}{\partial V} dV + \frac{\partial E}{\partial \dot{V}} d\dot{V} + \frac{\partial E}{\partial \mu_t} d\mu_t + \frac{\partial E}{\partial x} dx + \frac{\partial E}{\partial w} dw = 0 \tag{2}$$

Let us consider a perturbation dx of x around x_0 and the resulting perturbed state dV around V_0. The frequency formulation yields

$$x = x_0 + dxe^{i\omega t} \tag{3}$$

$$w = dwe^{i\omega t} \tag{4}$$

$$V = V_0 + dVe^{i\omega t} \tag{5}$$

$$\dot{V} = d\dot{V}e^{i\omega t} \tag{6}$$

$$\mu_t = \mu_{t_0} + d\mu_t e^{i\omega t} \tag{7}$$

with x_0, μ_{t0} and V_0 satisfying

$$E(V_0, 0, \mu_{t0}, x_0, 0) = 0 \tag{8}$$

Eqs. (3) and (5) yield

$$w = \frac{dx}{dt} = i\omega dxe^{i\omega t} \tag{9}$$

$$\dot{V} = \frac{dV}{dt} = i\omega dVe^{i\omega t} \tag{10}$$

Eqs (6) and (10) yield

$$d\dot{V} = i\omega dV \tag{11}$$

Eqs (4) and (9) yield

$$dw = i\omega dx \tag{12}$$

Eq. (2) can be written

$$\left(\frac{\partial E}{\partial V} + i\omega\frac{\partial E}{\partial \dot{V}}\right)dV + \frac{\partial E}{\partial \mu_t}d\mu_t + \left(\frac{\partial E}{\partial x} + i\omega\frac{\partial E}{\partial w}\right)dx = 0 \tag{13}$$

On the other side, the turbulence equations reads:

$$E_t\left(V_t, \dot{V}_t, V, \dot{V}, x, w\right) = 0 \tag{14}$$

with V_t the turbulent variables and

$$\mu_t = f(V_t, V) \tag{15}$$

The linearization of eqs. (14) and (15) gives to the first order:

$$\frac{\partial E_t}{\partial V_t} dV_t + \frac{\partial E_t}{\partial \dot{V}_t} d\dot{V}_t + \frac{\partial E_t}{\partial V} dV + \frac{\partial E_t}{\partial \dot{V}} d\dot{V} + \frac{\partial E_t}{\partial x} dx + \frac{\partial E_t}{\partial w} dw = 0 \tag{16}$$

$$d\mu_t = \frac{\partial f}{\partial V_t} dV_t + \frac{\partial f}{\partial V} dV \tag{17}$$

As previously, the frequency formulation gives

$$d\dot{V}_t = i\omega dV_t \tag{18}$$

Eq. (16) can be written

$$\left(\frac{\partial E_t}{\partial V_t} + i\omega \frac{\partial E_t}{\partial \dot{V}_t}\right) dV_t + \left(\frac{\partial E_t}{\partial V} + i\omega \frac{\partial E_t}{\partial \dot{V}}\right) dV + \left(\frac{\partial E_t}{\partial x} + i\omega \frac{\partial E_t}{\partial w}\right) dx = 0 \tag{19}$$

Eqs. (13), (19) and (17) lead to the following coupling system:

$$\begin{bmatrix} \frac{\partial E}{\partial V} + \frac{\partial E}{\partial \mu_t}\frac{\partial f}{\partial V} + i\omega\left(\frac{\partial E}{\partial \dot{V}} + \frac{\partial E_t}{\partial \dot{V}}\right) & \frac{\partial E}{\partial \mu_t}\frac{\partial f}{\partial V_t} \\ \frac{\partial E_t}{\partial V} & \frac{\partial E_t}{\partial V_t} + i\omega \frac{\partial E_t}{\partial \dot{V}_t} \end{bmatrix} \begin{bmatrix} dV \\ dV_t \end{bmatrix} = \begin{bmatrix} -\frac{\partial E}{\partial x} dx - i\omega \frac{\partial E}{\partial w} \\ -\frac{\partial E_t}{\partial x} dx - i\omega \frac{\partial E_t}{\partial w} \end{bmatrix} \tag{20}$$

All the operators appearing in eq. (20) have been obtained using an Automatic Differentiation tool, *TAPENADE* [4]. This tool provides the differentiated Fortran routines with respect to input variables prescribed by the user.

4 TRANSONIC WIND-TUNNEL CONFIGURATION

4.1 WTT configuration

4.1.1 WT flutter model

The experiments were carried out in the ONERA S2MA transonic wind tunnel. The test section of the wind tunnel is 1.75m x 1.77m. The model consists on a dummy half fuselage and a swept generic wing mounted on the wall. This wing/body configuration is shown in Figure 1.

The wing has a 10 % thick symmetrical airfoil section (NACA64A010 profile). The wing structure was designed to exhibit flutter involving a coupling between bending and torsion modes. This configuration has been chosen for its representativeness of an industrial configuration.

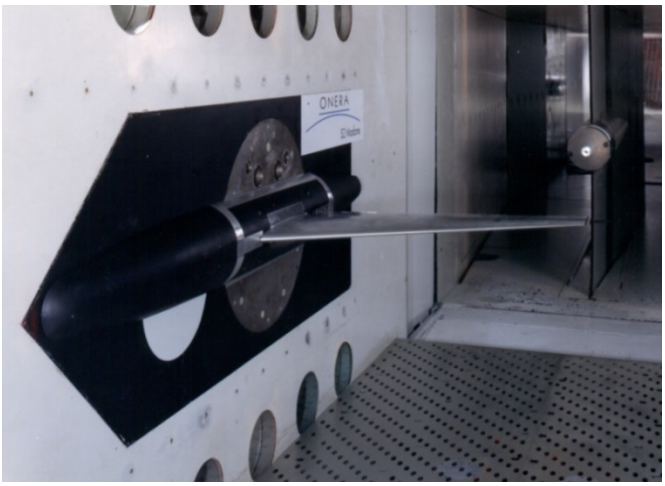

Figure 1: Generic horizontal tail configuration in S2-Modane wind tunnel

4.1.2 Aerodynamic modelling

The CAD model and the surface mesh used for the CFD computations are presented in Figure 2. The unstructured 3D mesh has 6.3 million nodes and 38 million tetrahedra. Unsteady non-linear and linearized Navier-Stokes computations are performed with the in-house code *AETHER*. The turbulence modelling is achieved through the Spalart-Allmaras model.

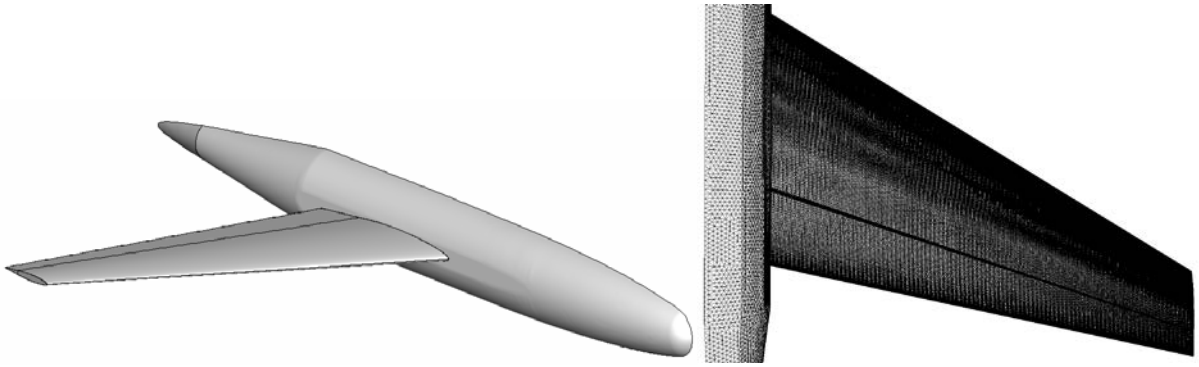

Figure 2: CAD Model and aerodynamic surface mesh

4.1.3 Structural modelling

A finite element model (Figure 3) of the WT flutter model is generated and tuned according to ground vibration tests. The boundary conditions are different depending on the test configuration (pressure test or flutter test).

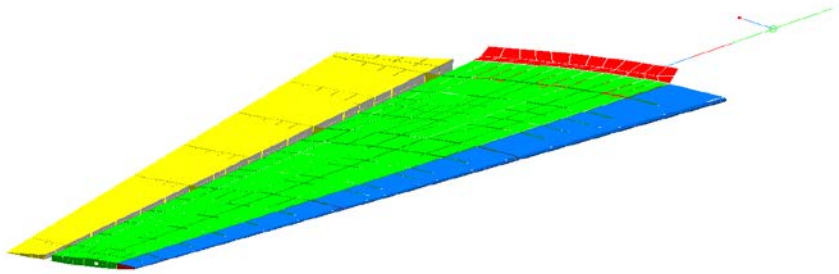

Figure 3: finite element model of the WT flutter model

4.2 Pressure configuration

The first part of the campaign was devoted to pressure tests (pressure configuration). The principle of these tests is to apply harmonic oscillations to the wing for different Mach number, angle of attack, frequency and forcing amplitude.

4.2.1 Subsonic domain

The first flow condition adressed on this test case is Mach 0.8 and AoA = 0°. In Figure 4 (bottom part) are illustrated both pressure (left) and boundary layer shape factor (right) parietal distributions. The flow is shock-less on the wing. In the top left part of the figure are shown the pressure sensitivities induced by a 30 % chord pitching motion for zero frequency in a 70% span section (third vertical black line in pressure and shape factor distributions). The three numerical results obtained with the Navier-Stokes solver (non-linear and linearized) are very similar to experimental data.

A zoomed-in view near the trailing edge (top right part) exhibits some differences between the Navier-Stokes computations. Taking into account the gradient of the viscous tensor, the pressure sensitivity to pitching motion is closer to experimental results near the trailing edge. The linearized solution with linearized turbulence also matches quite well the non-linear solution.

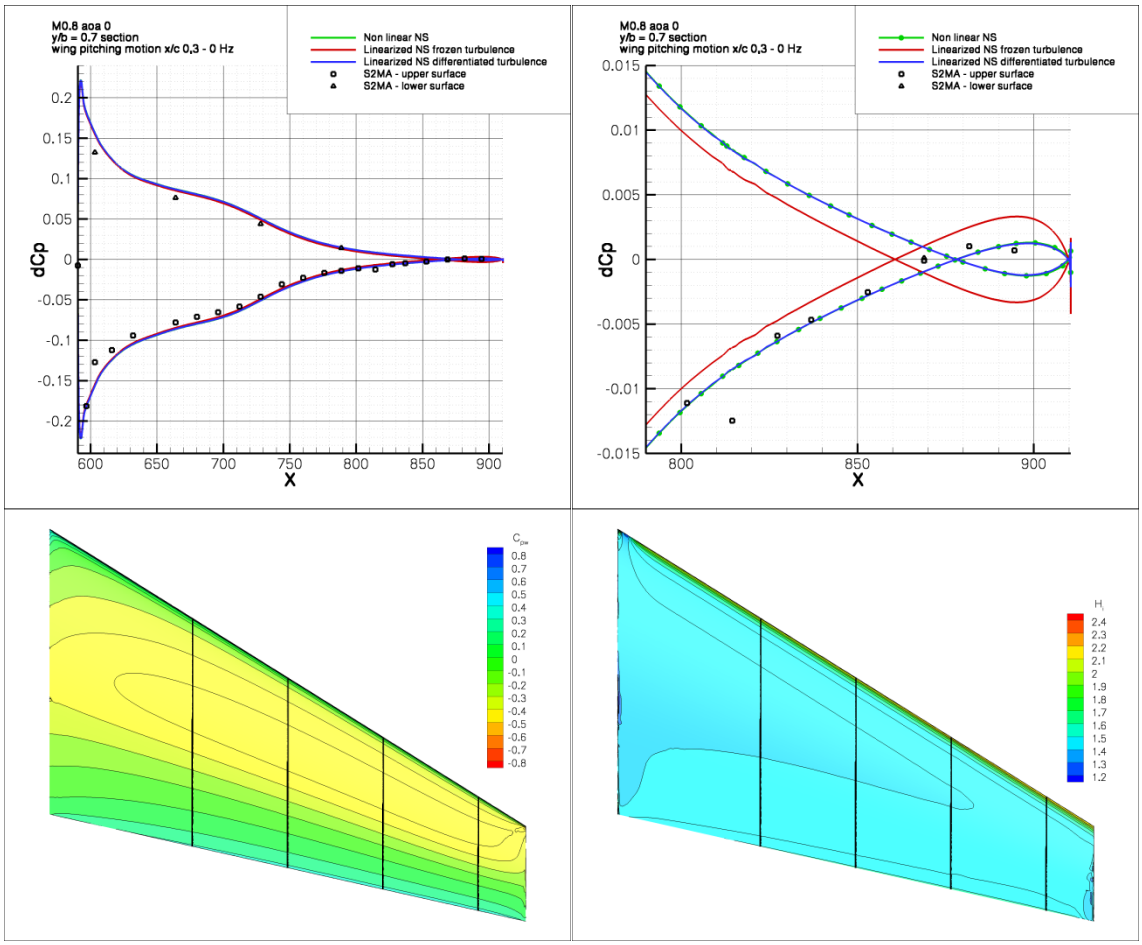

Figure 4: WT flutter model – M = 0.80 AoA = 0°

4.2.2 Transonic domain (attached flow)

In Figure 5 are presented results for Mach 0.85 AoA= 0° similar to those of the previous section. One can see on the bottom part of the figure that a shock appears in the outter part of the wing without any flow separation (Hi < 2.4). Excellent agreement between linearized computation and experimental data is obtained when taking into account linearized turbulence, especially near the trailing edge.

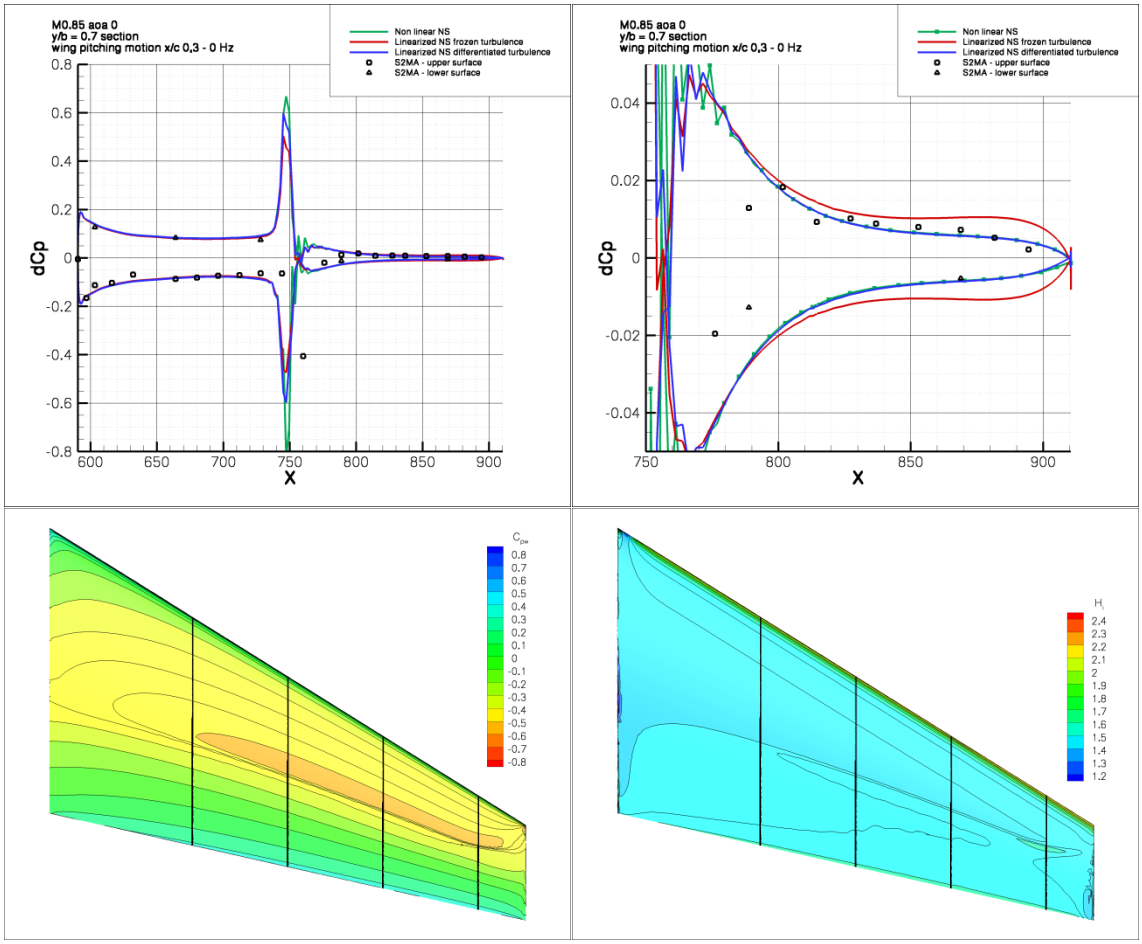

Figure 5: WT flutter model – M = 0.85 AoA = 0°

4.2.3 Transonic domain (separated flow)

Results for Mach 0.90 AoA= 0° are presented in Figure 6. This high transonic flow regime exhibits massive flow separation on the outer part of the wing (Hi > 2.4). Nonetheless, the linearized flow solver with linearized turbulence is able to converge and pressure sensitivity matches very well with the non-linear results.

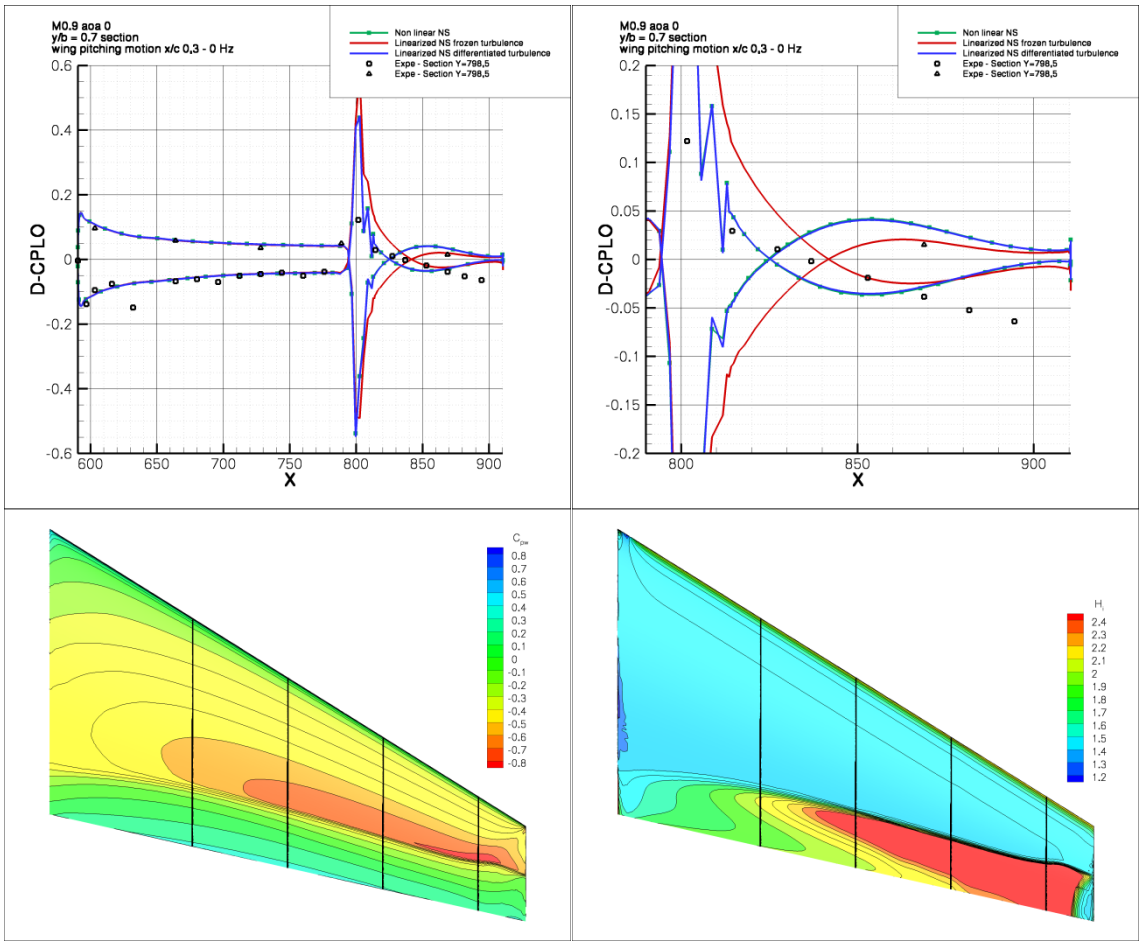

Figure 6: WT flutter model – M = 0.90 AoA = 0°

This flow condition also shows another benefit from taking into account turbulence gradients. Indeed, this approach improves the prediction of the aerodynamic behavior as shown previously but furthermore improves the efficiency of the linear system resolution. With frozen turbulence, the GMRES solver used in linearized Navier-Stokes computations does not succeed in reaching convergence. Adding turbulence gradients, the linear problem enables the solver to converge, and with the same convergence rate as for Mach 0.85.

4.2.4 Hinge moment sensitivity

In order to analyze in more detail the improvements introduced by differentiating turbulence in frequency-domain calculations, sensitivities of the hinge moment generated by pressure variations were computed. Figure 7 shows a comparison using only numerical data because experimental data were collected only for four wing sections and this sampling is too poor to derive a hinge moment.

Linearized frequency-domain Navier-Stokes solver with differentiated turbulence shows excellent agreement with non-linear time-domain calculations for a very large range of Mach numbers (from Mach 0.7 to 1.15), and achieving GMRES convergence is not a problem contrary to frozen turbulence.

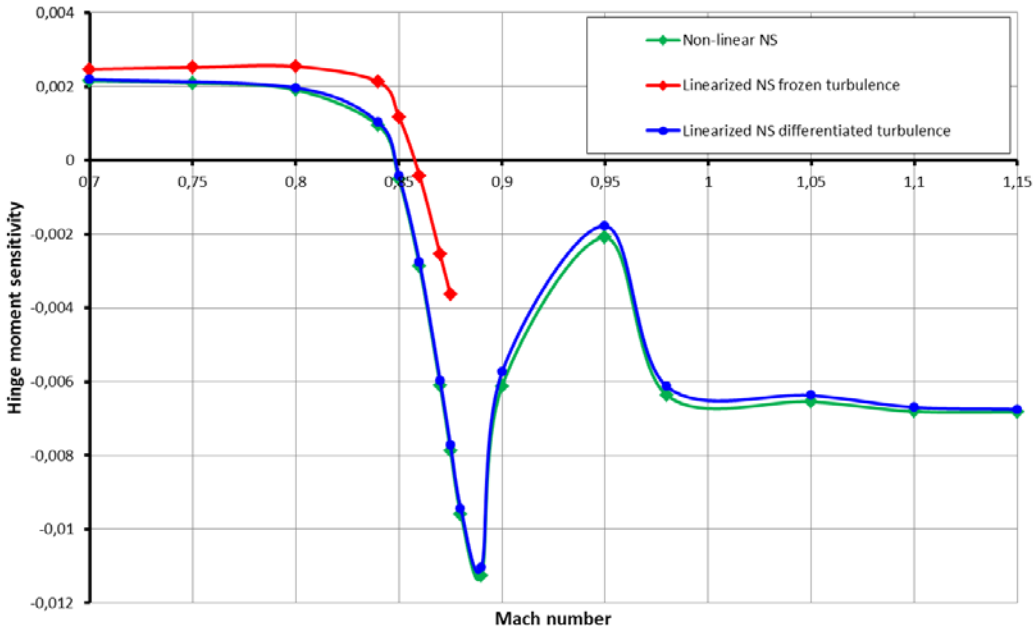

Figure 7: WT flutter model – AoA=0° − Hinge moment sensitivity vs. Mach number

4.3 Flutter configuration

A final validation of the frequency-domain linear solver was obtained by reproducing the WT flutter test using the linearized solver and the structural model presented in Section 4.1.3. A linear pressure database for a given displacement basis was generated and used as input for Generalized Aerodynamic Force (GAF) calculations in a flutter stability analysis based on the p-k method [5]. Flutter dynamic pressure function of Mach number is plotted in Figure 8 for both frozen and linearized turbulence and compared to experimental data. Good agreement with the experiment in the linearized turbulence case is observed, in particular for the prediction of the transonic dip. Freezing turbulence leads to a higher thus non-conservative value of the dip.

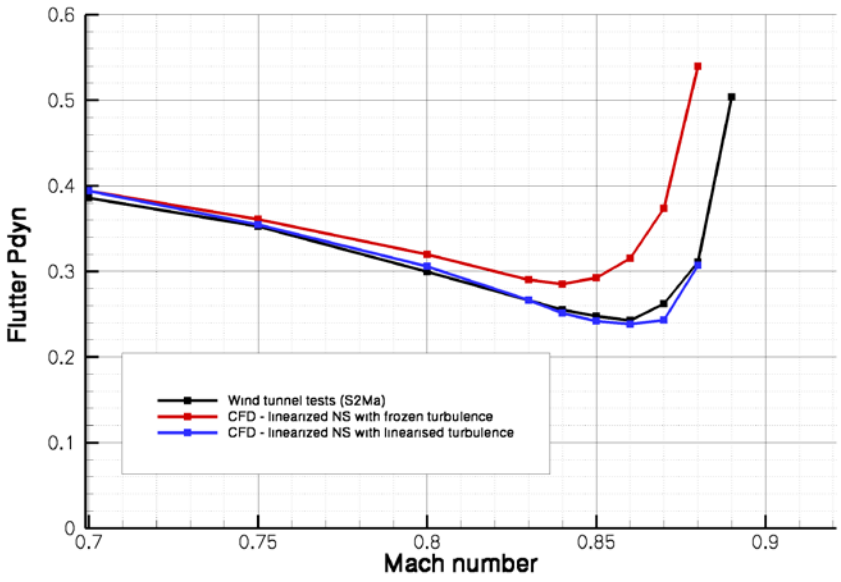

Figure 8: WT flutter model – AoA=0° − Flutter dynamic pressure vs. Mach number

5 INDUSTRIAL APPLICATIONS

The frequency-domain linearized Navier-Stokes solver with linearized turbulence described in the previous sections was applied to two aircraft configurations:

- Falcon 7X in a clean wing configuration
- Rafale fighter in an air-to-ground store configuration

5.1 Falcon 7X configuration

5.1.1 Test case presentation

The Falcon 7X configuration (half-aircraft) presented in Figure 9 is considered in the following analysis. The 3D mesh has 16.5 million nodes and 98.1 million tetrahedra. It is generated from an aircraft surface mesh having 198,000 nodes and 394,000 triangles. The steady flow condition around which the linear analysis is performed is Mach 0.97 and AoA=0.5°. This flight point corresponds to the maximum Mach number MD reached by this aircraft under high-speed dive flight testing for certification purpose. One can see in Figure 10 strong shock waves behind the cockpit, on the wing lower and upper surfaces and on the aft body, leading to flow separation as illustrated by the boundary layer shape factor shown in Figure 11.

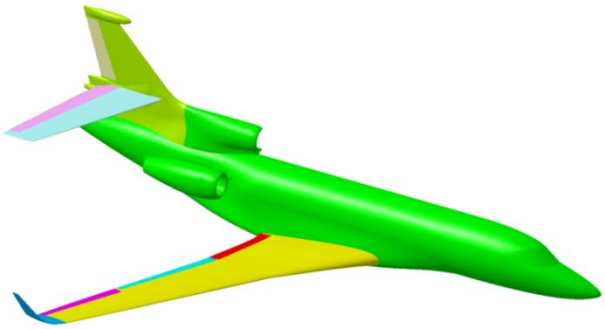

Figure 9: Falcon 7X configuration (half-aircraft)

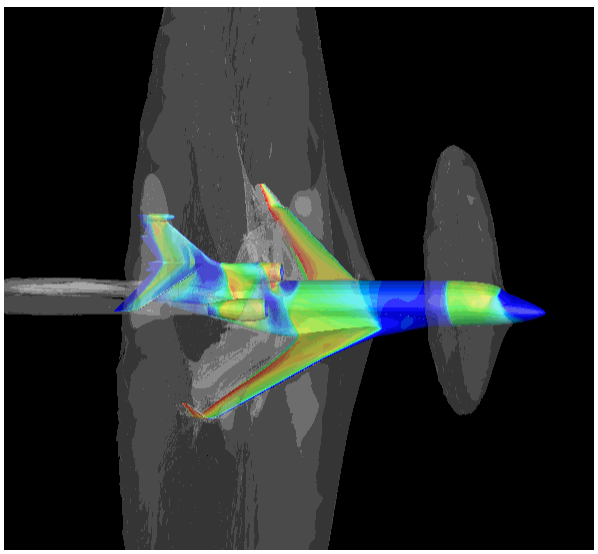

Figure 10: Falcon 7X – Mach 0.97 − Pressure and shock wave distributions

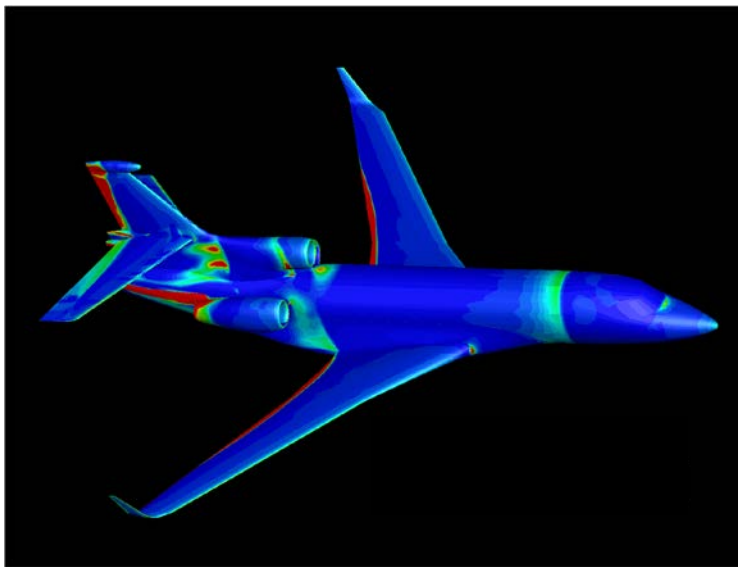

Figure 11: Falcon 7X – Mach 0.97 – Boundary layer shape factor (separated flow regions in red)

The structural mode shown in Figure 12 (essentially a wing bending mode) is considered as the displacement input to the linearized problem. An example of the resulting pressure coefficient sensitivity to this displacement on the lower side of the external wing and winglet is presented in Figure 13.

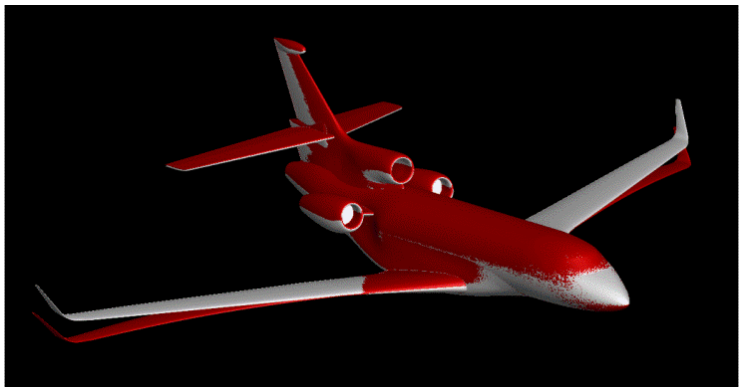

Figure 12: Falcon 7X – Structural mode displacement (in red, scaled) and rigid shape (in grey)

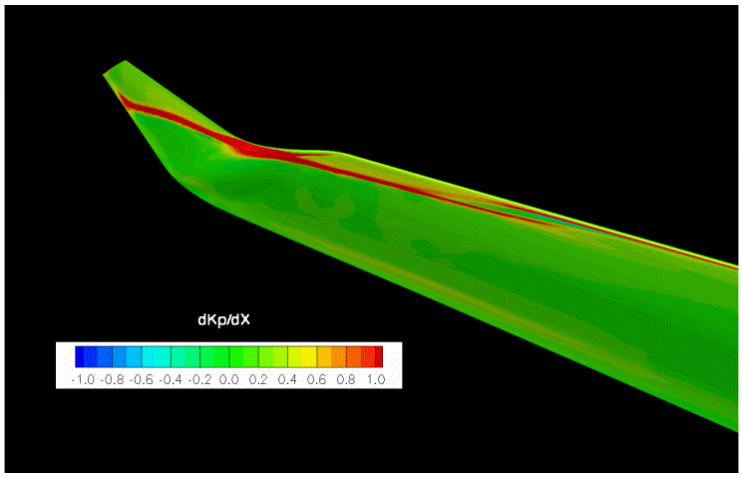

Figure 13: Falcon 7X – Mach 0.97 – Pressure coefficient sensitivity to modal displacement

5.1.2 Scalability study

In order to assess the computational performance of the parallel linearized Navier-Stokes solver, this 99 million-dof test case was run on an Intel Xeon-based bullx computing system ranging from 256 cores to 4096 cores with one subdomain per core. Convergence of the solver for all subdomain decompositions is presented in Figure 14. No degradation in the number of GMRES iterations required to converge the linear system to 10^{-5} w.r.t. the number of CPU cores is visible, contrary to what one would expect. This should however be analyzed on additional test cases before making a final conclusion on this behavior for this linearized solver.

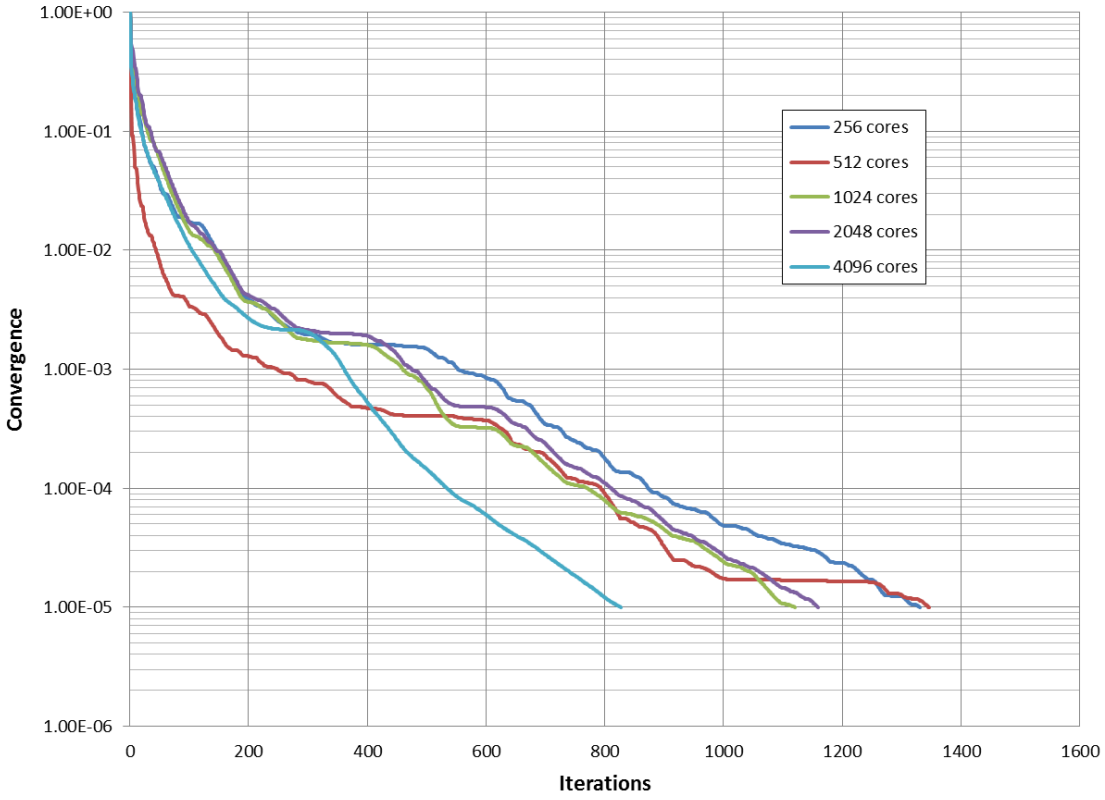

Figure 14: GMRES solver convergence for different subdomain decompositions

Computational efficiency of the parallel linear solver is synthetized in Figure 15 (speed-ups are scaled w.r.t. the 256-core timings) for the LHS matrix **A** and RHS vector **b** computation / assembly and for the GMRES solver applied to the **A x = b** linear problem. In order to present a fair comparison, the GMRES solver timings are scaled assuming the number of GMRES iterations required to converge the problem is the same for all subdomain decompositions (this assumes that GMRES timings are proportional to the number of matrix-vector products performed, which is the case based on our past experience).

Excellent scalability is achieved for both the LHS/RHS computation and for the GMRES solver, even for the 4096-core computing class leading to only 4,000 mesh nodes (or 24,000 dofs) per subdomain. Scalability higher than the theoretical value is obtained for the GMRES solver. This can be explained by the global cache size increase (summed over all CPU cores) as the number of subdomains increases, thus improving the computational efficiency of the preconditioner and iterative solver.

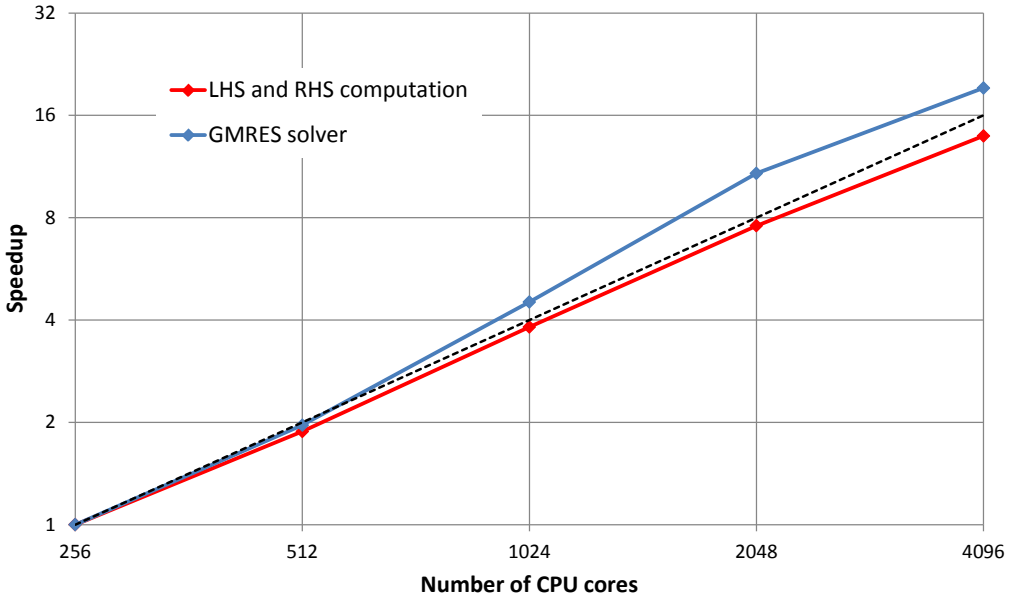

Figure 15: Falcon 7X modal displacement – Mach 0.97 – Linear solver scalability

Elapsed time (including IO) required to solve the linearized Navier-Stokes problem as a function of the number of CPU cores is presented in Figure 16. Elapsed time to solve this industrial-grade problem is 120 seconds on the 2048-core computing class.

Such a turnaround time for the linearized Navier-Stokes solver enables DASSAULT AVIATION to generate in about one month a linearized pressure database covering the aircraft flight domain and frequency requirements for a displacement basis sufficiently large to perform flutter analyses for all aircraft configurations (mass and center-of-gravity sensitivities).

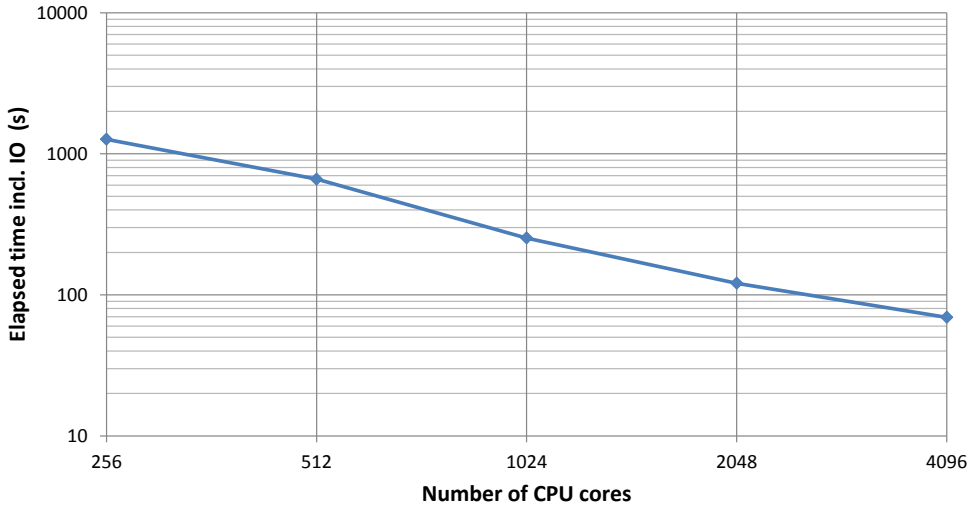

Figure 16: Falcon 7X modal displacement – Mach 0.97 – Linearized NS solver elapsed time

5.2 Rafale fighter configuration

The Rafale fighter in an air-to-ground configuration shown in Figure 17 is another industrial test case used to validate the robustness of our frequency-domain linearized Navier-Stokes solver. An effort has been put into taking into account the geometrical details of the stores (Figure 18) in the surface mesh (Figure 19) in order to capture their potential impact on the GAFs. The resulting aircraft surface mesh has 654,000 nodes and 1,307,000 triangles (for a half-aircraft configuration).

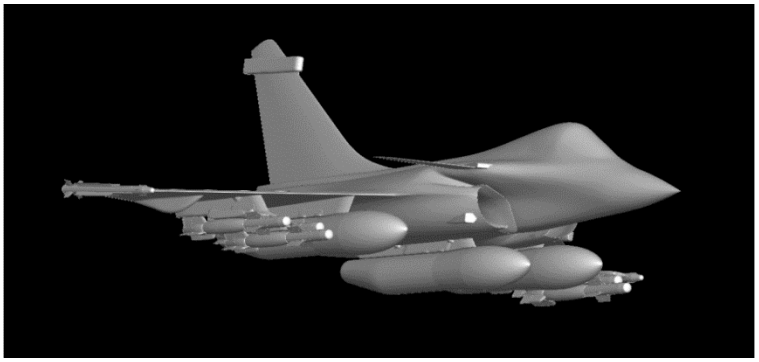

Figure 17: Rafale fighter configuration

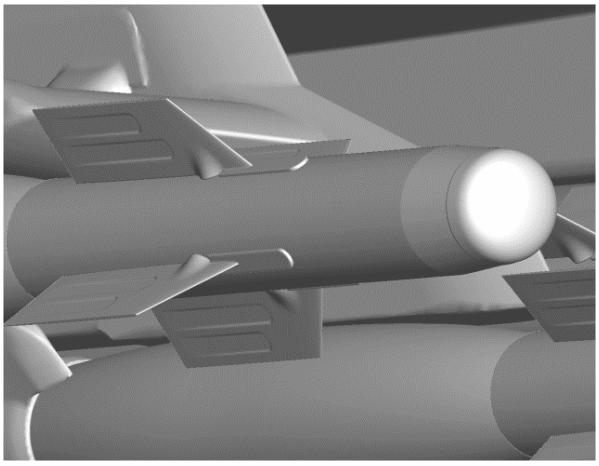

Figure 18: Rafale - store geometrical details

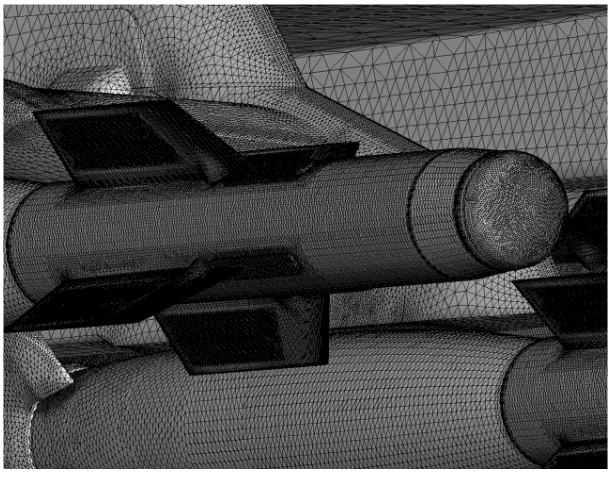

Figure 19: Rafale - store surface mesh

The 3D tetrahedral mesh has 30.5 million nodes and 180 million elements. Flight conditions for the steady flow computation are set to Mach 0.90 and AoA=3°. The resulting pressure field on the aircraft is presented in Figure 20 with some separated flow regions behind stores and pylons visible on the shape factor distribution in Figure 21.

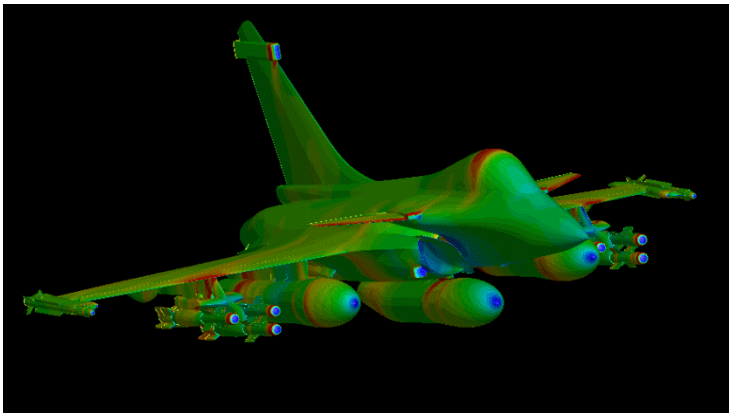

Figure 20: Rafale – Mach 0.90 − Pressure coefficient distribution

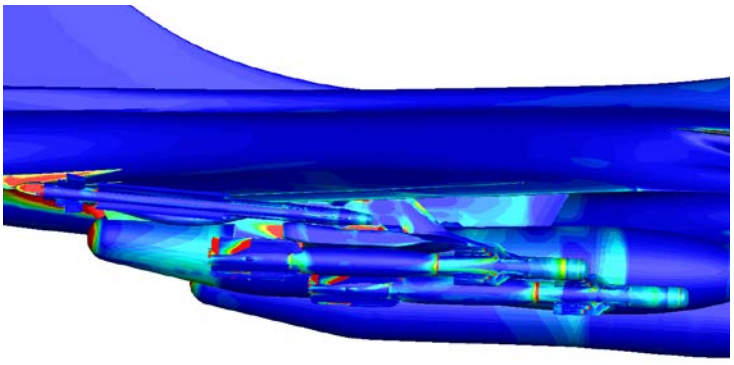

Figure 21: Rafale – Mach 0.90 – Shape factor distribution (separated flow regions in red)

The displacement considered for the analysis is shown in Figure 22. It is essentially a pitching oscillation of the tripod generating a pressure sensitivity on the stores (see Figure 23).

Figure 22: Rafale – Structural mode displacement (in green, scaled) and rigid shape (in grey)

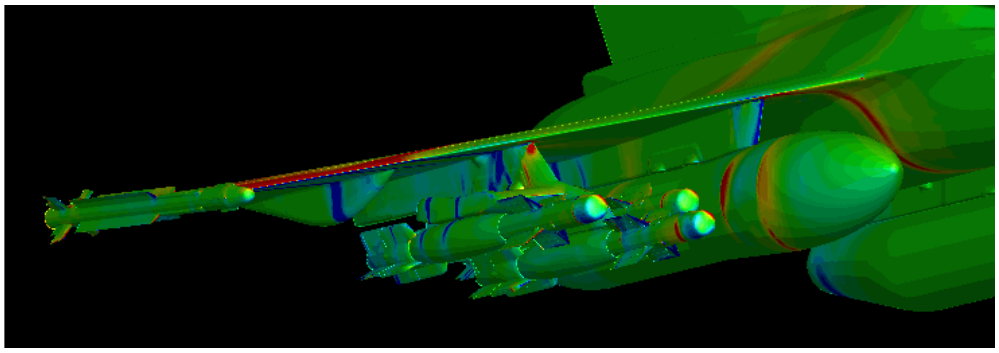

Figure 23: Rafale – Mach 0.90 – Pressure coefficient sensitivity to modal displacement

Convergence of the 183 million-dof linear system to 10^{-5} accuracy is obtained in 561 GMRES iterations (see Figure 24). Elapsed time (including IO) on a 2048-core computing class is 166 seconds, with 139 seconds spent in the GMRES solver. This test case clearly illustrates once again the robustness and efficiency of the frequency-domain linearized Navier-Stokes solver for industrial-type applications on large-scale computational meshes.

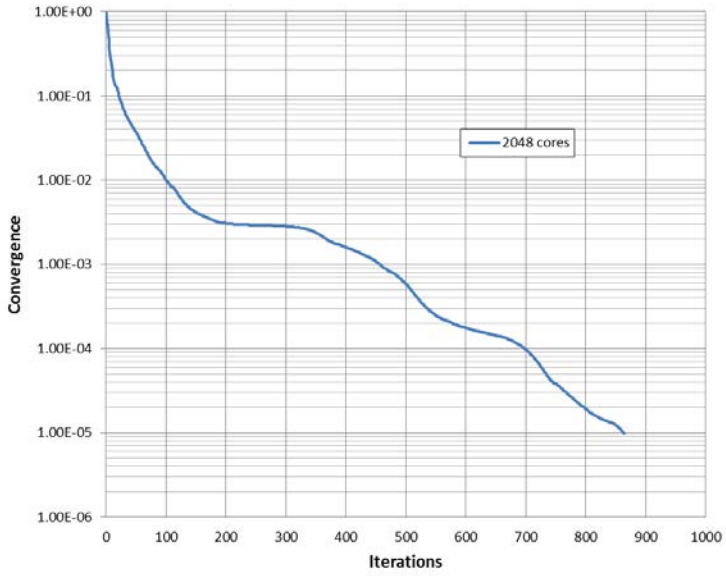

Figure 24: Rafale – GMRES solver convergence

6 CONCLUSION

A frequency-domain linearized Navier-Stokes solver taking into account linearized turbulence in a coupled form has been implemented in the DASSAULT AVIATION in-house *AETHER* finite element solver. An efficient and highly scalable preconditioned GMRES solver is used to solve the resulting linear system. Validation of the linearized solver has been performed on a wing-body configuration tested in ONERA S2MA wind tunnel in both pressure and flutter set-ups. Good agreement of linearized CFD pressure sensitivity to pitching motion with experimental data and non-linear Navier-Stokes results is obtained for different flow regimes ranging from subsonic to high transonic with separated flow regions. Numerical simulation of the flutter set-up and comparison to the experimental flutter results confirms the validation of the linearized solver.

Industrial-grade applications were performed on FALCON 7X and RAFALE fighter configurations leading to 100- to 200-million degree of freedom linear systems. Excellent scalability of the linearized solver leads to 2- to 3-minute turnaround times for the resolution of these systems of equations on a 2048-core HPC system. It is therefore possible to use this frequency-domain linearized Navier-Stokes solver in place of the DLM method with a substantial improvement in Generalized Aerodynamic Forces accuracy as its computing performance is now compatible with an aircraft program schedule.

Results presented in this paper use the Spalart-Allmaras model. On-going work will extend the method to other relevant turbulence models. Future developments will also be dedicated to extend our CFD capability to deal with non-linear flutter and LCO. Candidate techniques include HBM, POD or time-domain approaches. Flutter of laminar configurations will also require specific analysis.

7 ACKNOWLEDGEMENT

This work has been supported by a research program co-funded by the Direction Générale de l'Aviation Civile.

8 REFERENCES

[1] Industrial Use of Linearized CFD Tools for Aeroelastic Problems, F. Chalot, L. Daumas, N. Forestier & Z. Johan, *IFASD 2009-054*, Seattle.

[2] Harmonic Aerodynamics loads prediction including a linearized turbulence model, F. Chalot, L. Daumas, N. Forestier & V. Levasseur, *IFASD 2011-129*, Paris

[3] A Linearized Method for the Frequency Analysis of Three-Dimensional Fluid/Structure Interaction Problems in all Flow Regimes, M. Lesoinne, M. Sarkis, U. Hetmaniuk & C. Farhat, *Computational Methods Applied Mechanics Engineering*, Vol. 190, pp 3112-3140, 2001

[4] Software TAPENADE INRIA 2002, L. Hascouet, A. Dervieux and V. Pascual, developped by TROPICS project at the INRIA (Institut National de Recherche en Informatique et Automatique)

[5] Design for active flutter suppression and gust alleviation using state-space aeroelastic modeling, M. Karpel, 1982, *Journal of Aircraft*, 19(3), 221–227.

COPYRIGHT STATEMENT

The authors confirm that they, and/or their company or organization, hold copyright on all of the original material included in this paper. The authors also confirm that they have obtained permission, from the copyright holder of any third party material included in this paper, to publish it as part of their paper. The authors confirm that they give permission, or have obtained permission from the copyright holder of this paper, for the publication and distribution of this paper as part of the IFASD-2017 proceedings or as individual off-prints from the proceedings.